Cell Host & Microbe
Article

Linear Ubiquitination of NEMO Negatively Regulates the Interferon Antiviral Response through Disruption of the MAVS-TRAF3 Complex

S. Mehdi Belgnaoui,[1,2] Suzanne Paz,[1] Sara Samuel,[1,2] Marie-Line Goulet,[1] Qiang Sun,[1] Marjolein Kikkert,[4] Kazuhiro Iwai,[5] Ivan Dikic,[6] John Hiscott,[1,2,3,7,*] and Rongtuan Lin[1,2,3,*]
[1]Lady Davis Institute for Medical Research, Jewish General Hospital, Montreal, QC H3T 1E2, Canada
[2]Department of Microbiology and Immunology
[3]Department of Experimental Medicine
McGill University, Montreal, QC H3G 1Y6, Canada
[4]Department of Medical Microbiology, Center of Infectious Diseases, Leiden University Medical Center, 2300 RC Leiden, The Netherlands
[5]Department of Molecular and Cellular Physiology, Graduate School of Medicine, Kyoto University, Sakyo-ku, Kyoto 606-8501, Japan
[6]Institute of Biochemistry II, Goethe University School of Medicine, 60590 Frankfurt am Main, Germany
[7]Vaccine and Gene Therapy Institute, Port Saint-Lucie, FL 34987, USA
*Correspondence: jhiscott@vgtifl.org (J.H.), rongtuan.lin@mcgill.ca (R.L.)
http://dx.doi.org/10.1016/j.chom.2012.06.009

SUMMARY

The RIG-I/Mda5 sensors recognize viral intracellular RNA and trigger host antiviral responses. RIG-I signals through the adaptor protein MAVS, which engages various TRAF family members and results in type I interferon (IFNs) and proinflammatory cytokine production via activation of IRFs and NF-κB, respectively. Both the IRF and NF-κB pathways also require the adaptor protein NEMO. We determined that the RIG-I pathway is differentially regulated by the linear ubiquitin assembly complex (LUBAC), which consists of the E3 ligases HOIL-1L, HOIP, and the accessory protein SHARPIN. LUBAC downregulated virus-mediated IFN induction by targeting NEMO for linear ubiquitination. Linear ubiquitinated NEMO associated with TRAF3 and disrupted the MAVS-TRAF3 complex, which inhibited IFN activation while stimulating NF-κB-dependent signaling. In SHARPIN-deficient MEFs, vesicular stomatitis virus replication was decreased due to increased IFN production. Linear ubiquitination thus switches NEMO from a positive to a negative regulator of RIG-I signaling, resulting in an attenuated IFN response.

INTRODUCTION

The innate immune response represents the first line of defense against microbial pathogens and results in the production of immunomodulatory cytokines and the mobilization of innate immune cells. Central to the early host defense against viral infection is the production of interferons (IFN) and the synthesis of antiviral IFN stimulated genes (ISGs) that contain virus dissemination and activate the adaptive immune response (Liu et al., 2011; Sadler and Williams, 2008; Sen and Sarkar, 2007). Viral nucleic acids represent pathogen-associated molecular patterns (PAMPs) that are recognized by pattern recognition receptors (PRRs) to trigger the type I IFN—IFNα and IFNβ—production (Belgnaoui et al., 2011; Loo and Gale, 2011; Takeuchi and Akira, 2010; Yoneyama and Fujita, 2010). PRRs responsible for the detection of RNA viruses (and some DNA viruses) include both the membrane-bound Toll-like receptors (TLRs) and cytosolic sensors, such as retinoic acid-inducible gene-I (*RIG-I*)-like receptors (RLRs) (Belgnaoui et al., 2011; Beutler, 2009; Kumar et al., 2011; Loo and Gale, 2011; Takeuchi and Akira, 2010; Wilkins and Gale, 2010; Yoneyama and Fujita, 2010).

Early viral RNA replicative intermediates are mainly detected by RIG-I or Mda5 (melanoma differentiation-associated gene 5)—two characterized cytosolic viral RNA receptors belonging to the DExD/H box RNA helicase family (Kato et al., 2006; Yoneyama et al., 2004). The functions of RIG-I and Mda5 are nonredundant as RIG-I specifically detects intracellular double-stranded (ds) viral RNA bearing 5′ triphosphate and panhandle structures (Rehwinkel et al., 2010; Schlee and Hartmann, 2010; Schlee et al., 2009; Yoneyama and Fujita, 2008), leading to RIG-I interaction with the downstream adaptor protein MAVS (also known as Cardif/IPS-1/VISA) (Kawai et al., 2005; Meylan et al., 2005; Seth et al., 2005; Xu et al., 2005); Mda5 recognizes dsRNA structures such as synthetic poly (I:C) (>2 kb) and also signals through MAVS. Strategically localized at the outer mitochondrial membrane or on peroxisomes, MAVS assembles a signaling platform that triggers the IFN antiviral response, via activation of the transcription factors NF-κB and IFN regulator factors (IRF)-3 and -7 (Belgnaoui et al., 2011; Dixit et al., 2010; Scott, 2010). Crucial to MAVS complex formation and downstream signaling is the recruitment of the tumor necrosis ractor (TNF) receptor-associated factors (TRAFs), a family of cytoplasmic signaling adaptor proteins (Häcker et al., 2011). Several TRAF family members—TRAF-2, -3, -5 and -6—directly bind to MAVS via TRAF-interacting motifs (TIM) in the N- and C-terminal regions of MAVS (Paz et al., 2011; Saha et al., 2006; Tang and Wang, 2010; Xu et al., 2005). Interaction of MAVS with TRAF-2 or -6 is involved in IKK-dependent NF-κB activation (Xu et al., 2005), whereas TRAF3 is specifically

involved in TBK1-dependent IRF-3 or -7 activation (Paz et al., 2011; Saha et al., 2006).

In addition to the adapters, kinases, and accessory proteins of the MAVS complex, the NF-κB modulator protein NEMO (IKKγ) also interfaces with the RIG-I pathway and forms a regulatory bridge between the canonical IKKα/β kinases and the noncanonical kinases TBK1/IKKε via the TANK adaptor (Chariot et al., 2002; Zhao et al., 2007). NEMO activity is regulated by numerous posttranslational modifications, including ubiquitination, phosphorylation, and sumoylation (Liu and Chen, 2011; Sebban et al., 2006). Multiple ubiquitination signals have been identified—mono-, multiple- or polyubiquitination—that control protein fate and turnover (Bhoj and Chen, 2009; Dikic and Dötsch, 2009; Ikeda et al., 2010; Kirisako et al., 2006; Malynn and Ma, 2010; Weissman et al., 2011). Lys48 and Lys63 linkages are the best characterized types of polyubiquitination, with Lys48-linked polyubiquitination leading to ubiquitin-dependent degradation by the 26S proteasome (Dikic and Dötsch, 2009; Gallastegui and Groll, 2010). In contrast, Lys63-linked ubiquitination is associated with activation of protein kinases, protein-protein interactions, DNA repair, and endocytosis (Bergink and Jentsch, 2009; Bhoj and Chen, 2009).

Recently, another form of polyubiquitin chain formation was identified in association with NEMO; unlike Lys63- or Lys48-linked polyubiquitin chains that link ubiquitin moieties via a lysine residue of the previously attached ubiquitin, linear ubiquitination consists of head-to-tail linked ubiquitin moieties (Tokunaga et al., 2009). Upon TNFα stimulation, the E3 ligase linear ubiquitin chain assembly complex (LUBAC), composed of the two RING-IBR-RING (RBR)-containing E3 ligases, HOIL-1L (also known as RBCK1 and RNF54) and HOIP (also known as ZIBRA and RNF31), mediates the formation of linear ubiquitin chains on NEMO (Tokunaga et al., 2009), which functions to activate NF-κB signaling downstream of the TNF receptor. LUBAC activity is also dependent on a third accessory protein SHANK-associated RH domain interactor (SHARPIN) that stabilizes the E3 complex (Gerlach et al., 2011; Ikeda et al., 2011; Tokunaga et al., 2011).

Linear ubiquitination also modulates the RIG-I antiviral pathway but has not been reported to affect the Mda5 receptor. TRIM25, an E3 ligase that regulates RIG-I activation via Lys63-linked ubiquitination (Gack et al., 2007), was characterized as a unique target of the LUBAC complex (Inn et al., 2011), with linear ubiquitination of TRIM25 resulting in its proteasomal degradation. HOIL-1L or HOIP independently mediated Lys48-linked polyubiquitination and proteasomal degradation of TRIM25 (Inn et al., 2011).

In the present study, we demonstrate that the LUBAC complex contributes to negative regulation of the type I IFN response via linear ubiquitination of NEMO. Using chimeric forms of NEMO, modified by the addition of different linear ubiquitin moieties, we demonstrate that NEMO-Ub with two or more linear ubiquitin moieties, but not unmodified NEMO, bound to TRAF3 and dissociated the MAVS-TRAF3 complex. Furthermore, in SHARPIN-deficient *cpdm* mouse embryonic fibroblasts (MEFs), vesicular stomatitis virus (VSV) replication is decreased and the IFN antiviral response increased, highlighting the crucial role of linear ubiquitination in the negative regulation of the antiviral response.

RESULTS

LUBAC Inhibits the IFN Antiviral Response Downstream of the Adaptor MAVS

To examine the effect of linear ubiquitination on the antiviral response, LUBAC was coexpressed in HEK293 cells in the presence of NF-κB and IFN-stimulated response element (ISRE) reporter genes. LUBAC activated the NF-κB promoter more than 50-fold but inhibited Sendai virus (SeV)-mediated activation of the ISRE promoter by 3-fold (Figure 1A). To determine at what level in the pathway LUBAC blocked ISRE expression, the active CARD domain containing form of RIG-I (ΔRIG-I) (Yoneyama et al., 2004), the Mda5 sensor, MAVS, TBK1 kinase, or the active form of IRF-3 (IRF-3[5D]) were expressed in the presence or absence of LUBAC. All expression constructs resulted in a 300- to 1000-fold induction of ISRE-Luc reporter activity (Figure 1B; white bar). ISRE activation driven by Mda5, ΔRIG-I, or MAVS was inhibited more than 85% by LUBAC, whereas ISRE induction by TBK1 or IRF-3(5D) was not affected by LUBAC coexpression (Figure 1B; compare black to white bars). The same expression constructs also induced ISG15 protein expression (Figure 1C; compare lanes 3, 5, 7, 9, and 11), and the addition of LUBAC inhibited ISG15 induction by Mda5, ΔRIG-I, or MAVS (Figure 1C; lanes 4, 6, and 8), but not by TBK1 or IRF-3 (5D) (Figure 1C, lanes 10 and 12). To confirm the inhibitory effect of LUBAC on IFN signaling, expression of HOIL-1L was knocked down by small-interfering RNA (siRNA) in A549 cells, followed by SeV challenge for 4, 8 and 12 hr. IRF-3 phosphorylation (4 hr) and subsequent degradation (12 hr) was increased in cells with decreased levels of HOIL-1L (Figure 1D). Inhibition of HOIL-1L expression also led to an increase in ISRE promoter activation by Mda5, ΔRIG-I, or MAVS, but not by TBK1 or IRF-3 (5D) (Figure 1E). Similar experiments using the TLR3 and TLR4 adaptor protein TRIF demonstrated that LUBAC did not affect MAVS-independent ISRE promoter activation (data not shown). These results indicate that LUBAC inhibits the IFN antiviral response downstream of MAVS and upstream of TBK1.

Linear Ubiquitination of NEMO Inhibits IFN Induction

The association of the IKK adaptor NEMO and the TBK1 adaptor TANK coordinately regulates NF-κB and IRF-3 signaling downstream of RIG-I (Chariot et al., 2002; Zhao et al., 2007). To investigate whether LUBAC-mediated linear ubiquitination of NEMO was involved in the control of type I IFN signaling, we generated NEMO chimeric constructs fused at their C terminus with linear ubiquitin chains of variable sizes, consisting of one, two, or four linear ubiquitin moieties, termed NEMO-Ub1, NEMO-Ub2, and NEMO-Ub4, respectively. The different NEMO-Ub chimeras stimulated NF-κB reporter gene activity without any additional stimulation, whereas unmodified wild-type NEMO (WT-NEMO) failed to activate the NF-κB reporter gene (Figure 2A). When the chimeric constructs were tested with the ISRE promoter after SeV infection or expression of Mda5, ΔRIG-I, MAVS, TBK1, or IRF-3(5D), neither WT-NEMO nor NEMO-Ub chimeras activated the ISRE promoter alone; in contrast, NEMO-Ub2 and NEMO-Ub4 inhibited SeV, Mda5, ΔRIG-I, or MAVS-driven promoter activity by >75%, compared to WT-NEMO or NEMO-Ub1 (Figures 2B and 2C). Similar to the results obtained with

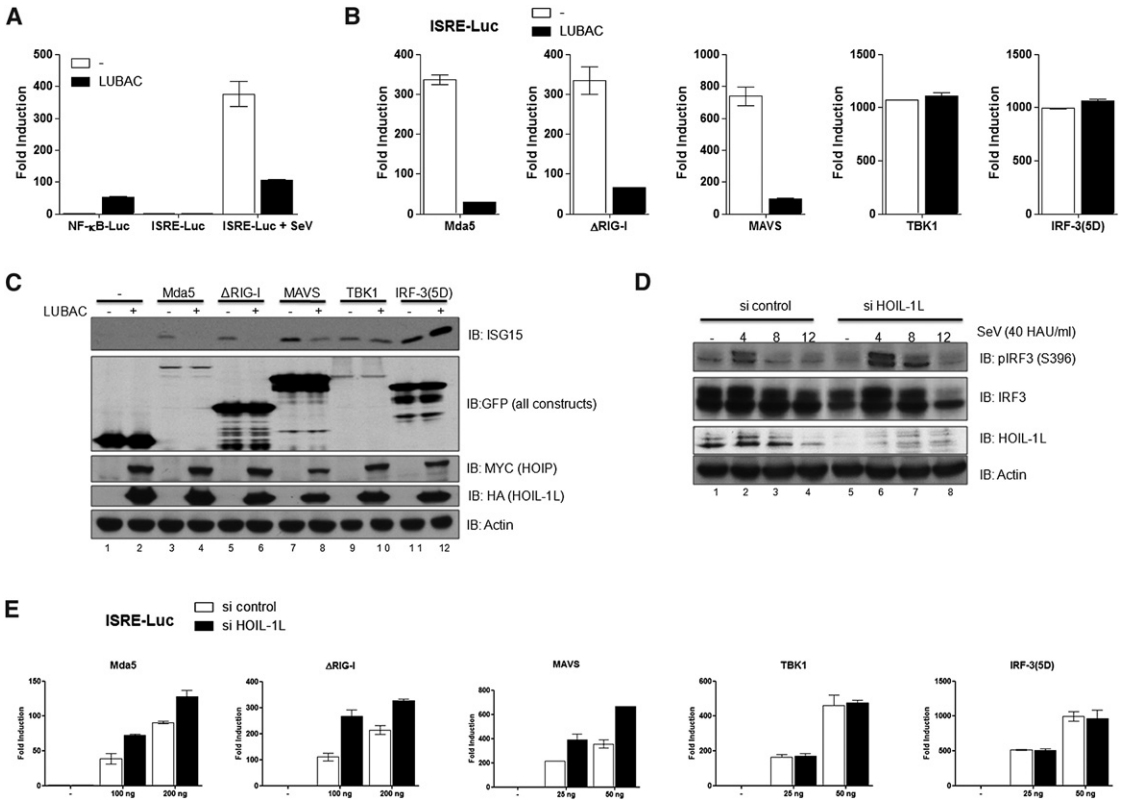

Figure 1. LUBAC Inhibits the IFN Response Downstream of MAVS

(A) HEK293 cells were transfected with either the NF-κB-Luc or ISRE-Luc promoter along with empty vector or LUBAC and were left untreated or challenged with SeV for 16 hr. Luciferase activity was analyzed at 24 hr posttransfection and fold activation was determined compared to empty vector; values represent the average ± SD. Results are representative of at least three experiments run in triplicate.

(B) HEK293 were challenged with either SeV or the following activators encoding, Mda5 (200 ng), ΔRIG-I (200 ng), MAVS (50 ng), TRIF (50 ng), TBK1 (50 ng), or IRF-3 (5D) (50 ng), along with either empty vector (–) or LUBAC (400 ng) and the ISRE-Luc reporter plasmids. Luciferase activity and analysis was performed as in (A).

(C) HEK293 were transfected with empty vector (–), GFP-Mda5, GFP-ΔRIG-I, GFP-MAVS, GFP-TBK1, or GFP-IRF-3(5D), with or without LUBAC. Whole-cell lysates were subjected to immunoblot analysis and blotted with anti ISG15 (top panel), anti-GFP (second panel), anti-MYC (third panel), anti-HA (fourth panel), or anti-actin (last panel) antibodies.

(D) A549 cells transfected with either siRNA control (si control) or siRNA HOIL-1L (si HOIL-1L) then left untreated or treated with SeV for 4, 8, or 12 hr. Immunoblot analysis was performed using either anti p-s396-IRF-3 antibody (top panel), anti-IRF3 antibody (second panel), anti-HOIL-1L antibody (third panel), or anti-actin antibody (bottom panel).

(E) HEK293 cells were transfected with either siRNA control or siRNA against HOIL-1L. At 48 hr posttransfection, cells were again transfected with the ISRE-Luc promoter along with empty vector or Mda5, ΔRIG-I, MAVS, TBK1, IRF-3(5D). Luciferase activity was monitored as in (A) and (B); values represent the average ± SD.

LUBAC, the NEMO-Ub constructs did not inhibit TBK1- or IRF-3(5D)-driven ISRE activity. MAVS-independent activation of the ISRE promoter by TRIF was not affected by the different NEMO-Ub constructs (data not shown). Furthermore, NEMO-Ub2 inhibited expression of various ISGs—ISG15, ISG56 and RIG-I—whereas WT-NEMO or NEMO-Ub1 had no effect on ISG expression (Figure 2D; compare lane 5, 8, and 11—top, second, and third panels). Interestingly, NEMO-Ub2 also failed to inhibit ISG expression after IFNα treatment (Figure 2D; lane 12), suggesting that the inhibition of the type I IFN signaling pathway occurred at an early stage of signaling, prior to IFN release.

Linear Ubiquitinated NEMO Interacts with TRAF3

Because both TRAF3 and NEMO are positive regulators of type I IFN signaling downstream of MAVS, we investigated the possibility that linear ubiquitination of NEMO regulated the formation of the MAVS-TRAF3 complex. In coprecipitation experiments, TRAF3 coprecipitated with NEMO-Ub2, weakly with NEMO-Ub1 (Figure 3A; compare lane 4 to 3, top panel), and not with WT-NEMO (Figure 3A; lane 2, top panel). Next, NEMO and TRAF3 were expressed in the presence or absence of LUBAC. NEMO alone did not interact with TRAF3, but the addition of LUBAC led to the formation of the NEMO-TRAF3 complex (Figure 3B; compare lane 5 to 6, second panel). In the same experiment, using a NEMO-specific antibody, modified forms of NEMO were detected in the presence of LUBAC, thus suggesting that linear ubiquitinated NEMO interacted with TRAF3 (Figure 3B; lane 6—top panel). To demonstrate that LUBAC E3 ligase complex formation was required for this interaction, HOIL-1L and/or HOIP were expressed in the presence of

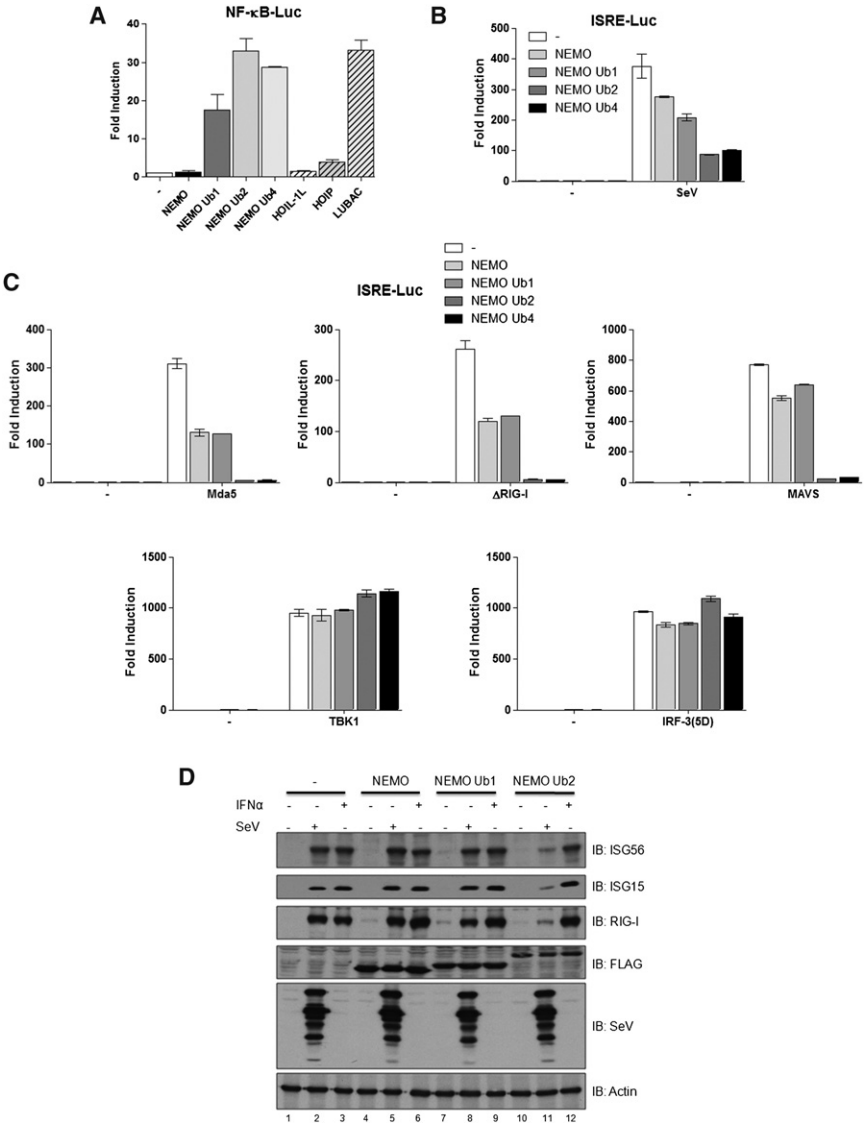

Figure 2. Linear Ubiquitination of NEMO Inhibits IFN Induction

(A) HEK293 cells were transfected with empty vector (–), NEMO, NEMO-Ub1, NEMO-Ub2, NEMO-Ub4, HOIL-1L, HOIP, or LUBAC along with the NF-κB-Luc reporter plasmid. Luciferase activity was analyzed as described in Figure 1A; values represent the average ±SD.

(B and C) HEK293 cells were challenged with either SeV or the following activators—Mda5 (200 ng), ΔRIG-I (200 ng), MAVS (50 ng), TRIF (50 ng), TBK1 (50 ng), or IRF-3 (5D) (50 ng)—along with either empty vector (–), NEMO-Ub1, NEMO-Ub2, or NEMO-Ub4 (400 ng each) and the ISRE-Luc reporter plasmids. Luciferase activity was analyzed as in (A); values represent the average ± SD.

(D) HEK293 cells were either treated or not with IFNα (16 hr); infected or not with SeV (12 hr); and transfected with either empty vector (–), NEMO, NEMO-Ub1, or NEMO-Ub2. Whole-cell lysates were subjected to immunoblot analysis using anti-ISG56 (top panel), anti-ISG15 (second panel), anti-RIG-I (third panel), anti-FLAG (fourth panel), anti-SeV (fifth panel), or anti-actin (last panel) antibodies.

TRAF3 and NEMO (Figure 3C). A NEMO-TRAF3 interaction was readily detected when both LUBAC components were present, but not when individual components were expressed (Figure 3C; compare lane 7 to lanes 8 and 9), thus demonstrating that NEMO-TRAF3 interaction was dependent on the presence of the LUBAC complex.

Linear Ubiquitinated NEMO Competes with MAVS for TRAF3 Binding

To examine whether linear ubiquitination of NEMO affected IFN signaling at the level of MAVS-TRAF3 interaction, MAVS-TRAF3 association was determined in the presence of LUBAC and/or NEMO. Expression of MAVS led to an interaction with TRAF3 (Figure 4A; lane 4); when individually expressed, NEMO and LUBAC coexpression modestly disrupted this interaction by 2.4- and 1.7-fold, respectively (59% and 41%, respectively) (Figure 4A; lane 5 and 7), but in the presence of both LUBAC and NEMO, the MAVS-TRAF3 complex was decreased more than 5-fold (81%) (Figure 4A; lane 8). Conversely, the LUBAC-induced TRAF3-NEMO interaction was disrupted in the presence of MAVS (Figure 4B; compare lanes 8 and 9) and the reciprocal coprecipitation generated similar results (Figure 4C). To determine whether linear ubiquitinated NEMO and MAVS compete for TRAF3 binding, NEMO was precipitated in the presence of constant amounts of LUBAC and TRAF3, but increasing amounts of MAVS. Increasing MAVS disrupted the LUBAC-induced NEMO-TRAF3 complex in a dose-dependent manner (Figure 4D). Taken together, these results indicate that the MAVS-TRAF3 interaction is disrupted by linear ubiquitinated NEMO.

Increased Antiviral Response and Decreased VSV Replication in *cpdm* MEFs

To test the endogenous role of linear ubiquitination in the RIG-I pathway, *cpdm* MEFs, deficient in the accessory protein SHARPIN that functions to stabilize the LUBAC complex (Gerlach et al., 2011; Ikeda et al., 2011; Tokunaga et al., 2011), were used to measure replication of a recombinant VSV expressing green fluorescent protein (VSV-GFP) (Figure 5A). In *cpdm* MEFs, at 24 and 48 hr after VSV infection, fewer cells were positive for GFP fluorescence, compared to WT MEFs (~70% GFP-positive WT MEFs, compared to ~40% GFP-positive *cpdm* MEFs) (Figure 5B). Additionally, VSV replicated in *cpdm* compared to WT MEFs, as reflected by VSV glycoprotein (VSV-G) expression (Figure 5C; second panel). Furthermore, an enhanced antiviral response was observed in *cpdm* MEFs

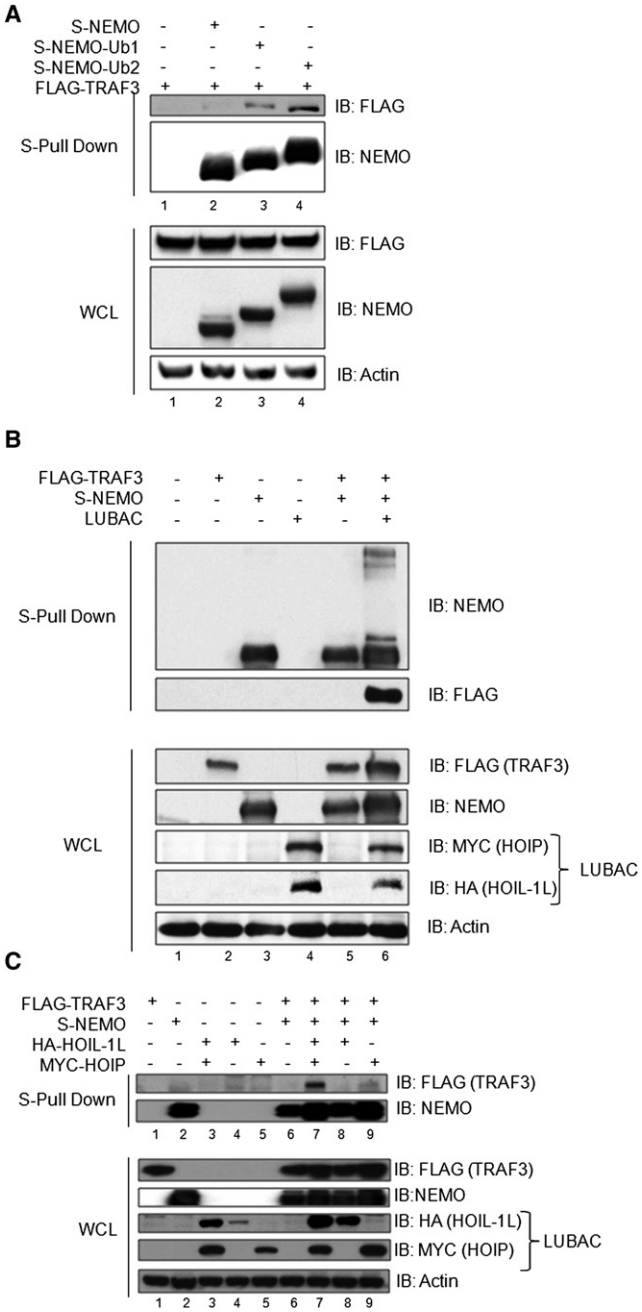

Figure 3. Linear Ubiquitinated NEMO Interacts with TRAF3

(A) HEK293 cells were transfected with FLAG-tagged TRAF3 and an empty vector or S-tagged WT-NEMO (S-NEMO), S-NEMO-Ub1, or S-NEMO-Ub2. S-tagged proteins were then precipitated using the S-tag purification technique and immunoblotted using anti FLAG antibody (top panel) to reveal TRAF3 interaction. Equal pull-down of NEMO was verified using anti NEMO antibody (second panel). Whole-cell lysates were subjected to immunoblot analysis using anti FLAG (third panel, TRAF3), anti-NEMO (fourth panel) or anti-actin (last panel) antibodies.

(B) HEK293 cells were transfected with S-NEMO, FLAG-TRAF3, S-NEMO, and FLAG-TRAF3 or S-NEMO and FLAG-TRAF3 in combination with HOIL-1L and HOIP (LUBAC). S-NEMO was pulled down as in (A) and immunoblotted using anti-NEMO (first panel, pull-down control) or anti-FLAG (second panel, TRAF3 interaction). Whole-cell lysates were subjected to immunoblot analysis using anti FLAG (third panel, TRAF3), anti-NEMO (fourth panel), anti-MYC (fourth panel, HOIL-1L), anti-HA (fifth panel, HOIP) or anti-actin (last panel) antibodies.

(C) HEK293 cells were transfected with S-NEMO, FLAG-TRAF3, S-NEMO, and FLAG-TRAF3 or S-NEMO and FLAG-TRAF3 in combination with HOIL-1L alone, HOIP alone, or with both (LUBAC). S-NEMO was pulled down and immunoblotted as in (B). Whole-cell lysates were subjected to immunoblot analysis using the same antibodies as in (B).

compared to WT MEFs following VSV infection, as reflected by an increase in IFNβ promoter activity (~200-fold induction in WT MEFs compared to ~600-fold increase in *cpdm* MEFs) and IFNα4 promoter (~50-fold induction in WT MEFs compared to ~250-fold in *cpdm* MEFs) (Figure 5D). RIG-I protein expression was also increased in *cpdm* MEFs, thus demonstrating a stronger induction of IFN production (Figure 5C; top panel). Because NF-κB activation by TNFα was shown to be impaired in *cpdm* MEFs (Gerlach et al., 2011; Ikeda et al., 2011; Tokunaga et al., 2011), we also examined whether NF-κB activation was defective in the context of VSV infection. NF-κB and IL6 promoter activation were attenuated in *cpdm* MEFs after VSV infection (from ~20-fold to ~5-fold and from ~9-fold to ~3-fold respectively) (Figure 5E). Because SHARPIN was shown to have an antiapoptotic role upon TNFα activation (Gerlach et al., 2011; Ikeda et al., 2011), the level of apoptosis in WT and *cpdm* MEFs was assessed after virus infection. An increase in apoptosis, as measured by Annexin V/ propidium iodide (PI) positive cells (45% in *cpdm* MEFs compared to 15% in WT MEFs), and an accumulation of cleaved caspase 3 in *cpdm* compared to WT MEFs were detected (Figures 5F and 5G), demonstrating that SHARPIN deficiency rendered the cells more sensitive to virus-induced cell death.

Linear Ubiquitinated NEMO Interacts with TRAF3 and Dissociates the MAVS-TRAF3 Complex

Next, using a linear ubiquitin chain-specific antibody (Tokunaga et al., 2009), we demonstrated that endogenous NEMO was targeted for linear ubiquitination after VSV infection (Figure 6A). In WT MEFs, NEMO was linearly ubiquitinated 48 hr after infection (Figure 6A; top panel, lane 5), concomitant with its interaction with TRAF3 (Figure 6A; second panel, lane 5). In contrast, NEMO did not undergo linear ubiquitination in *cpdm* MEFs and did not bind TRAF3 (Figure 6A; lanes 6–10, top and second panels). The reciprocal coimmunoprecipiation experiment in which TRAF3 was immunoprecipitated confirmed the strong interaction between TRAF3 and NEMO at 48 hr in WT MEFs (Figure 6B). This association was decreased by more than 6-fold in *cpdm* MEFs, indicating that TRAF3-NEMO association was enhanced in a linear ubiquitin-dependent manner (Figure 6B; compare lane 5 to 10). In parallel, an increased association of MAVS-TRAF3 was observed in *cpdm* MEFs compared to WT MEFs, particularly at 48 hr after infection (~5-fold increase) (Figure 6C; compare lane 5 to 10), arguing that linearly ubiquitinated NEMO dislodges TRAF3 from MAVS by physical interaction. This dissociation from MAVS did not occur when NEMO was not linearly ubiquitinated.

The expression of antiviral IFN stimulated genes—*IRF7, DDX58* (RIG-I), and *OAS1*—were also highly induced in *cpdm* MEFs (Figure 7A; black bars) after virus infection, compared to WT MEFs (white bars), due to intact signaling as a consequence

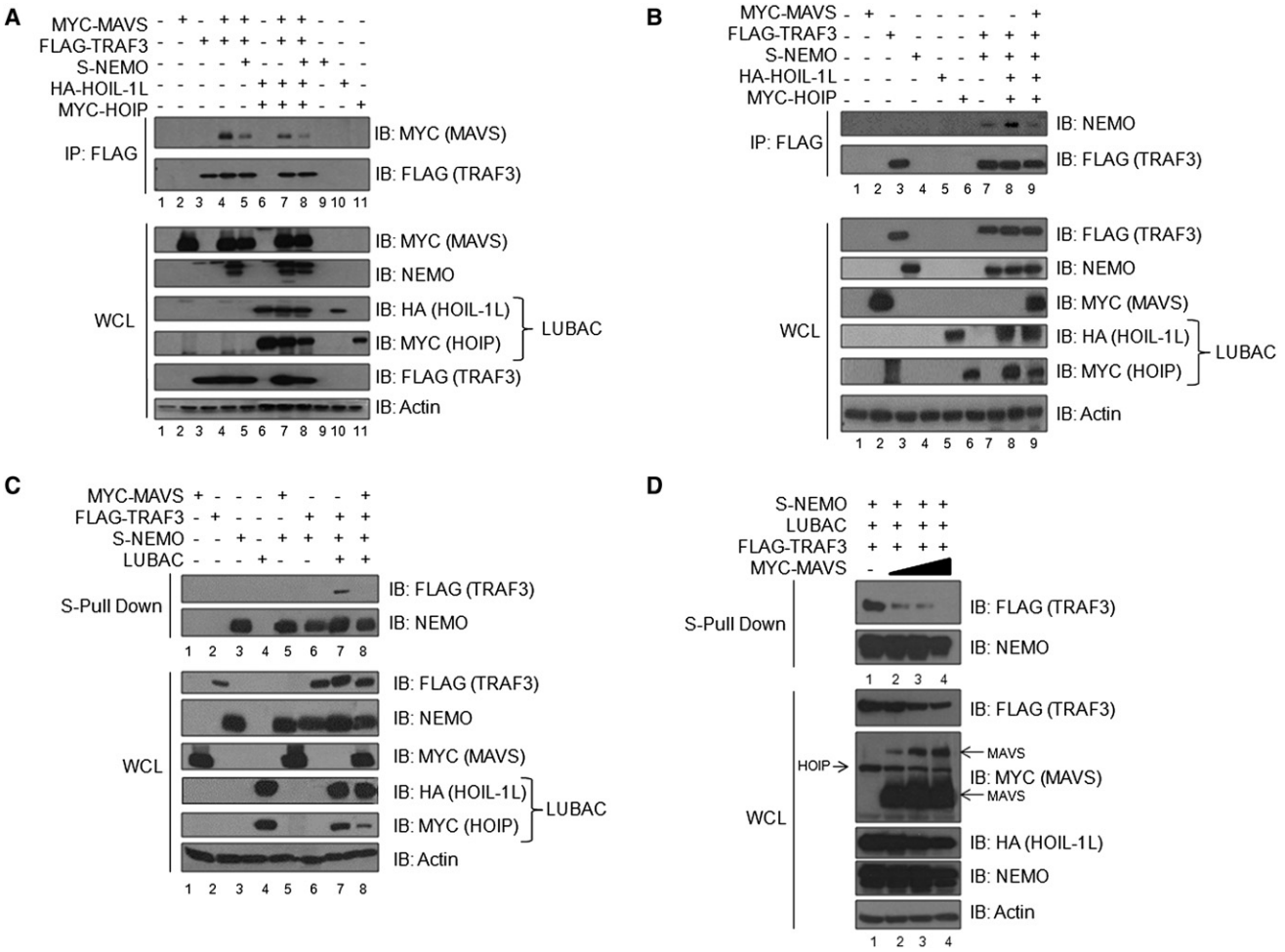

Figure 4. Linear Ubiquitinated NEMO Competes with MAVS for TRAF3 Binding

(A and B) HEK293 cells were transfected with MYC-MAVS, S-NEMO, FLAG-TRAF3, HA-HOIL-1L, MYC-HOIP in combination or alone. FLAG-TRAF3 was immunoprecipitated using an anti-FLAG antibody and subjected to immunoblot analysis using an anti-MYC antibody (A) to detect MAVS interaction (top panel) or anti-NEMO (B) (top panel). FLAG antibody was used to probe for immunoprecipitated TRAF3 (second panel). Whole-cell lysates were subjected to immunoblot analysis using anti-MYC (MAVS and HOIP), anti-NEMO, anti-HA (HOIL-1L), anti-FLAG (TRAF3), and anti-actin (eighth panel) antibodies.

(C) HEK293 cells were transfected with MYC-MAVS, S-NEMO, FLAG-TRAF3, and LUBAC in combination or alone. S-NEMO was precipitated and immunoblot analysis was performed using FLAG antibody to detect TRAF3 interaction (top panel). Precipitated NEMO was revealed using anti-NEMO antibody (second panel). Whole-cell lysates were subjected to immunoblot analysis using anti-FLAG (third panel, TRAF3), anti-NEMO (fourth panel), and anti-MYC (fifth panel, MAVS; and seventh panel, HOIP), anti-HA (sixth panel, HOIL-1L), and anti-actin (eighth panel) antibodies.

(D) HEK293 cells were transfected with S-NEMO, FLAG-TRAF3, and LUBAC with an increasing amount of MYC-MAVS. S-NEMO was precipitated and immunoblot analysis was performed using FLAG antibody to detect TRAF3 interaction (top panel). Precipitated NEMO was revealed using anti-NEMO antibody (second panel). Immunoblots using anti-FLAG (third panel, TRAF3), anti-MYC (fourth panel, MAVS and HOIP), anti-HA (fifth panel, HOIL-1L), anti-NEMO (sixth panel), and anti-actin (seventh panel) antibodies.

of MAVS-TRAF3 complex formation in *cpdm* MEFs (Figure 6C). *IRF7* mRNA levels peaked at ~150-fold in *cpdm* MEFs compared to ~15-fold in WT MEFs; similarly, DDX58 peaked at ~13-fold and OAS1 peaked at ~250-fold; the values in WT MEFs were ~3-fold and ~30-fold, respectively. By ELISA, a 3-fold increase in IFNα and IFNβ release into the supernatant of *cpdm* cells was detected compared to WT MEFs (Figure 7B). Strikingly, VSV infection of *cpdm* MEFs failed to induce *IL6* promoter (Figure 7C; black bars), illustrating the functional impact of NF-κB inhibition on inflammatory cytokine gene expression. IL6 release post-VSV infection was also 3-fold lower in *cpdm* compared to WT MEFs (Figure 7D). Altogether, these results demonstrate that linear ubiquitination of NEMO following virus infection facilitates the formation of a NEMO-TRAF3 heterodimer; sequestration of TRAF3 away from the MAVS complex contributes to the termination of RIG-I dependent signaling (Figure 7E). Linear ubiquitination of NEMO thus negatively regulates production of type I IFN and multiple ISGs, while positively regulating activation of NF-κB and inflammatory gene expression.

DISCUSSION

In the present study, we demonstrate an essential role for LUBAC-mediated linear ubiquitination of NEMO in the

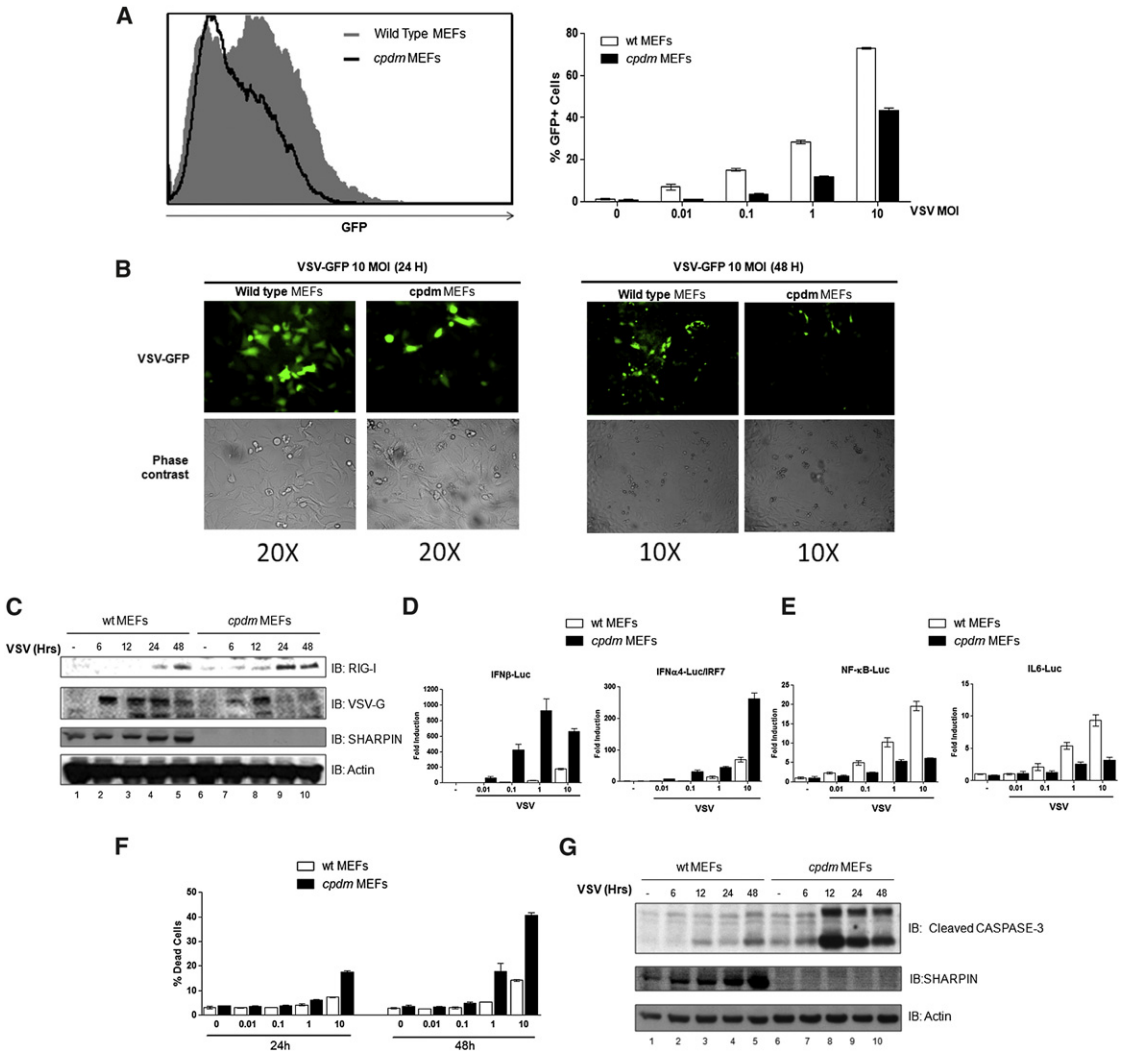

Figure 5. Increased Antiviral Response and Decreased VSV Replication in *cpdm* MEFs

(A) VSV-GFP infection was assessed using flow cytometry in *cpdm* and WT MEFs 24 hr following virus infection with different MOIs (0, 0.01, 0.1, 1, and 10). The histogram represents GFP expression in WT and *cpdm* MEFs at 10 MOI. Two-way ANOVA $p < 0.0001$; values represent the average ± SEM.

(B) Fluorescent (top panel) and phase contrast microscopy (bottom panel) of WT and *cpdm* MEFs infected with VSV-GFP at 10 MOI for 24 hr (magnification ×20) or 48 hr (magnification ×10).

(C) WT and *cpdm* MEFs were infected with VSV (10 MOI) for the indicated times. Whole-cell lysates were subjected to immunoblot analysis using anti-RIG-I (top panel), anti-VSV (second panel), anti-SHARPIN (third panel), and anti-actin (bottom panel) antibodies.

(D and E) WT and *cpdm* MEFs were transfected with the IFNβ, IFNα4 + IRF7, IL6, or NF-κB reporter and infected with VSV at 8 hr posttransfection. Luciferase activity was analyzed at 24 hr posttransfection and fold activation was determined compared to empty vector; values represent the average ± SD.

(F) WT and *cpdm* MEFs infected with VSV-GFP with the indicated MOI for 24 hr or 48 hr. Apoptosis was measured by flow cytometry by Annexin V/PI staining; values represent the average ± SEM.

(G) WT and *cpdm* MEFs were infected with VSV (10 MOI) for the indicated times. Whole-cell lysates were subjected to immunoblot analysis using anti-cleaved caspase 3 (top panel), anti-SHARPIN (second panel) and anti-actin (bottom panel) antibodies.

negative regulation of the RIG-I antiviral pathway through sequestration of TRAF3 from the MAVS adaptor. LUBAC and NEMO-Ub constructs inhibited RIG-I signaling downstream of MAVS and upstream of TBK1; linearly ubiquitinated NEMO interacted physically with TRAF3 and disrupted the MAVS-TRAF3 complex, thus providing a mechanistic explanation for the downregulation of RIG-I signaling. Using SHARPIN-deficient *cpdm* MEFs, we observed, on the one hand, an increased and prolonged antiviral response, while on the other hand, an impaired NF-κB activation, indicating that linear ubiquitination is required for NF-κB activation downstream of RIG-I. Interestingly, an increase in apoptotic cell death was also detected in SHARPIN-deficient *cpdm* MEFs after VSV infection, potentially attributable to the absence of the antiapoptotic activity of NF-κB.

These studies reveal a negative feedback mechanism used by host cells to regulate the IFN antiviral response. The formation of the MAVS-TRAF3 complex is a crucial step of the IFN response

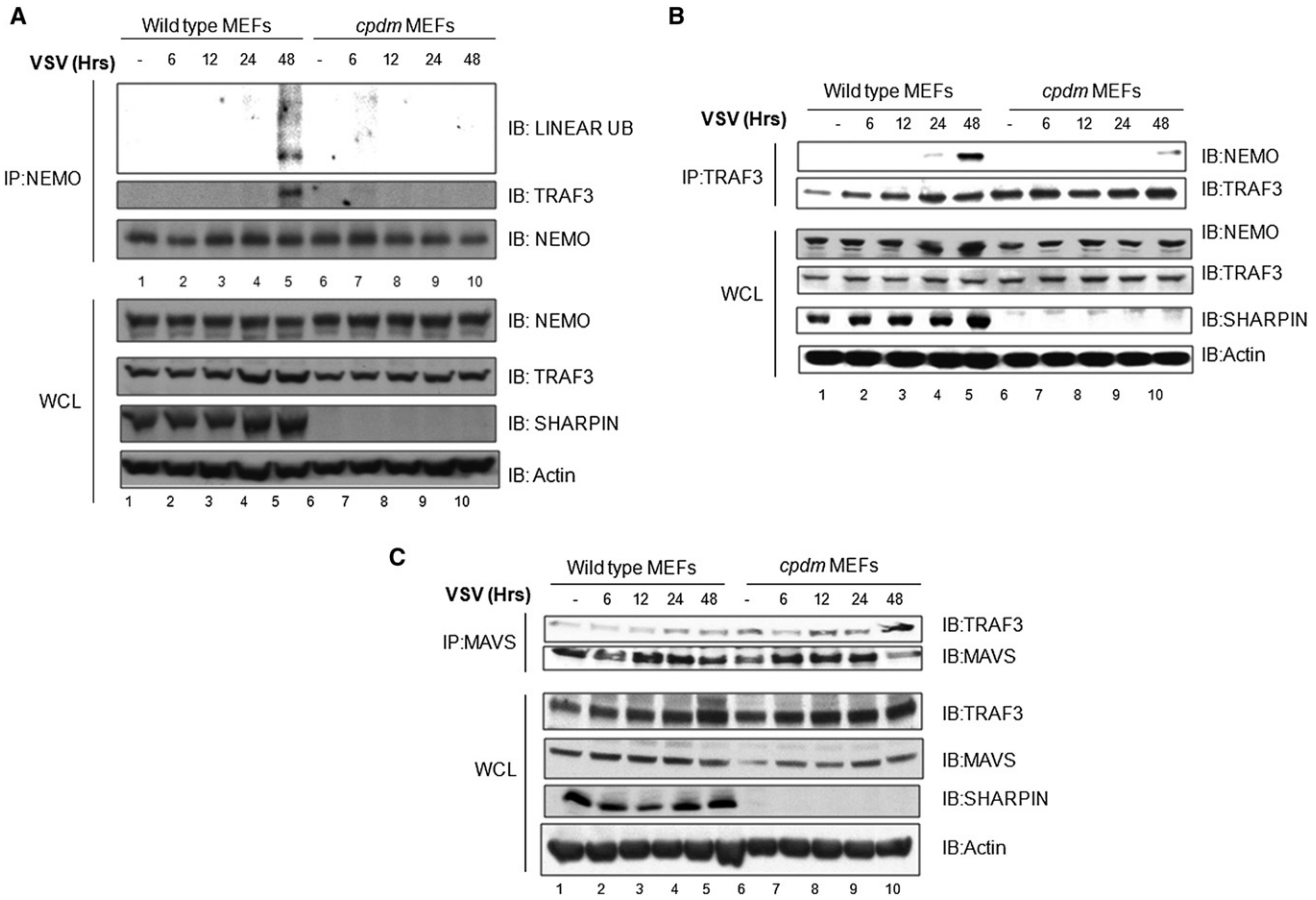

Figure 6. Linear Ubiquitinated NEMO Interacts with TRAF3 and Dissociates MAVS-TRAF3

(A) WT and *cpdm* MEFs were infected with VSV (10 MOI) for the indicated times. Endogenous NEMO was immunoprecipitated using an anti-NEMO antibody, and its linear ubiquitination status as well as its ability to interact with TRAF3 was assessed using anti-linear ubiquitin (top panel) and anti-TRAF3 (second panel) antibodies. Equal amounts of immunoprecipitated NEMO were revealed using an anti-NEMO antibody (third panel). Input amounts for NEMO, TRAF3, SHARPIN, and actin are shown (last four panels).

(B) WT and *cpdm* MEFs were infected with VSV (10 MOI) for the indicated times. Endogenous TRAF3 was immunoprecipitated using an anti-TRAF3 antibody, and its ability to interact with NEMO was assessed using anti-NEMO antibody (top panel). Equal amounts of immunoprecipitated TRAF3 were revealed using an anti-TRAF3 antibody (second panel). Input for NEMO, TRAF3, SHARPIN, and actin are shown (last four panels).

(C) WT and *cpdm* MEFs were infected with VSV (10 MOI) for the indicated times. Endogenous MAVS was immunoprecipitated using an anti-MAVS antibody, and its ability to interact with TRAF3 was assessed using anti-TRAF3 antibody (top panel). Equal amounts of immunoprecipitated MAVS were revealed using an anti-MAVS antibody (second panel). Input amounts for TRAF3, MAVS, SHARPIN, and actin are shown (last four panels).

to RNA viruses, and early after virus infection, TRAF3 acts as bridging adaptor in the assembly of the active MAVS-TRAF3-TBK1 signaling complex that also includes NEMO (Paz et al., 2011; Zeng et al., 2010). Previously, we demonstrated the positive regulatory role of NEMO as a bridge between the canonical IKKα/β kinases and the noncanonical kinases TBK1/IKKε via the TANK adaptor (Zhao et al., 2007). Here, we show that at 24–48 hr postinfection, linear ubiquitination of NEMO by LUBAC facilitates its interaction with TRAF3, an association that sequesters TRAF3 away from MAVS (Figure 7E). Linear ubiquitination thus switches NEMO from a positive mediator of RIG-I signaling to a negative regulator that dissociates the antiviral signaling complex through a competition mechanism. There are several possibilities that may explain the increased ability of linear ubiquitinated NEMO to dissociate TRAF3 from MAVS, including a direct binding of TRAF3 to linear ubiquitin chains or a high affinity of TRAF3 for the conformationally altered form of NEMO.

Regulation of RIG-I signaling through ubiquitination has been extensively studied. TRIM25 and RNF135 (REUL) activate the pathway by mediating Lys63-linked polyubiquitination of RIG-I (Gack et al., 2007; Oshiumi et al., 2010). Conversely, inhibition of the pathway is achieved through the Lys48-linked polyubiquitination and subsequent proteasomal degradation of RIG-I and MAVS by RNF125, and TRAF3 by Triad3A (Arimoto et al., 2007; Nakhaei et al., 2009). The ubiquitin-editing protein A20 and several deubiquitinases such as DUBA, OTUB, and CYLD also negatively regulate RIG-I signaling (Kayagaki et al., 2007; Li et al., 2010; Lin et al., 2006; Wertz et al., 2004; Zhang et al., 2008b); CYLD was shown to inhibit RIG-I signaling by removing Lys63-linked ubiquitin chains from both RIG-I and TBK1 (Zhang et al., 2008b), while DUBA inhibits the pathway by cleaving

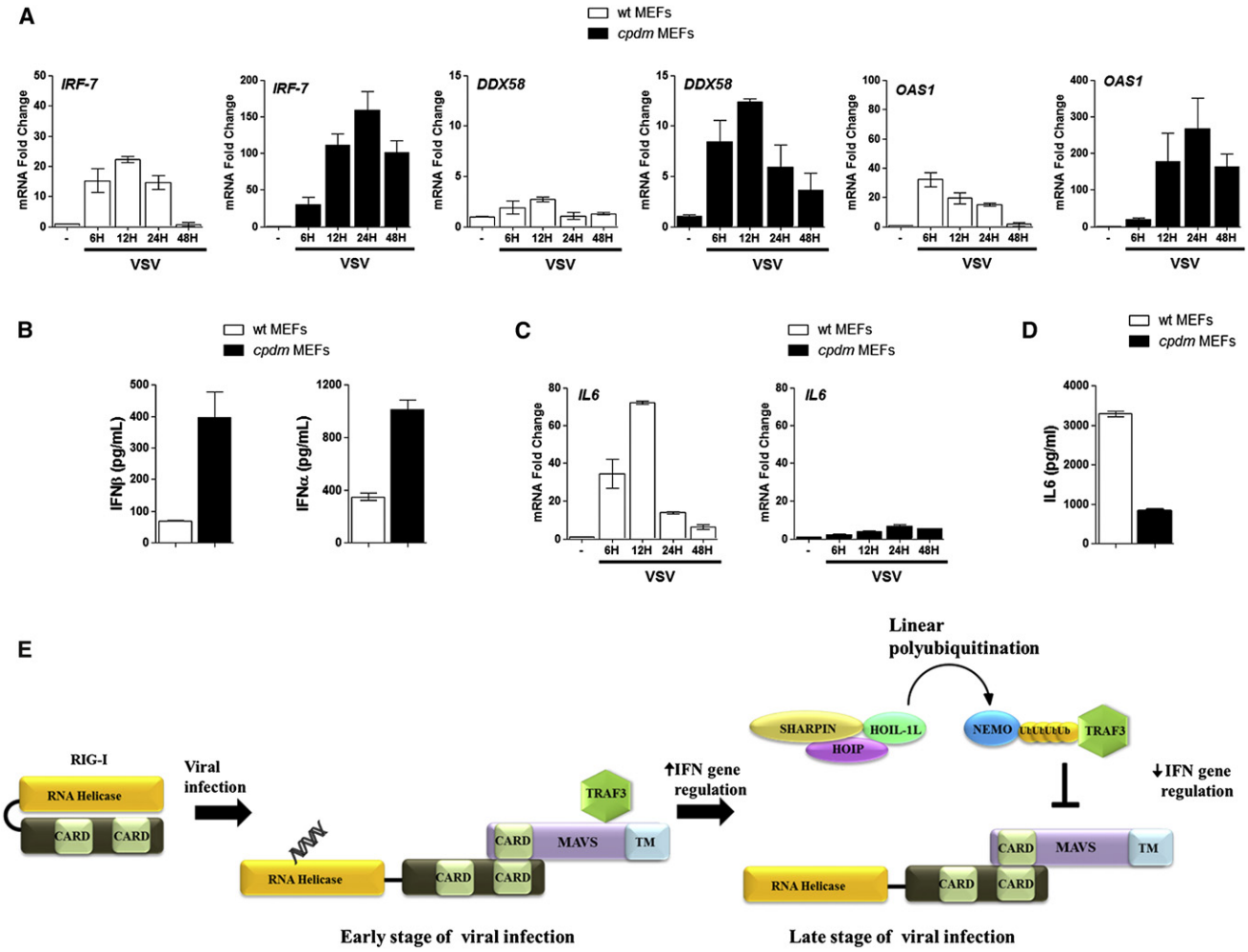

Figure 7. Increased IFN Response following Virus Infection in *cpdm* MEFs

(A–D) qPCR analysis of total RNA isolated from WT and *cpdm* MEF cells. Relative fold-expression levels of *IRF7*, *DDX58* (RIG-I), *OAS1* (A), and *IL6* (C) versus *GAPDH* mRNA are shown. Data are representative of at least two experiments run in duplicate; values represent the average ± SD. In (B) and (D), ELISA of IFNα, IFNβ B), and IL6 (D) in the supernatant of WT and *cpdm* MEFs infected with VSV at 10 MOI for 48 hr. Data are representative of two experiments run with three individual samples; values represent the average ± SEM.

(E) A schematic of the inhibition of RIG-I signaling by linear ubiquitinated NEMO-mediated dissociation of the MAVS-TRAF3 complex.

Lys63 chain from TRAF3, leading to its dissociation from TBK1 (Kayagaki et al., 2007).

These multiple nonredundant mechanisms of regulation of the early antiviral response illustrate the requirement to maintain appropriate regulatory homeostasis of the IFN pathway. Many examples of the pathological consequences of dysregulation of antiviral and inflammatory responses to pathogens exist. The *IFIH1* gene encoding Mda5 has been associated with several types of autoimmune diseases such as type I diabetes, Grave's disease, and systemic lupus erythematous (SLE) (Gateva et al., 2009; Smyth et al., 2006; Sutherland et al., 2007). Activation of TLR7 and TLR9 on B cells and plasmacytoid dendritic cells by self-nucleic acid is also crucial step in SLE pathogenesis (Barrat and Coffman, 2008; Guiducci et al., 2010). Production of TLR-mediated antinuclear antibodies and type I interferon correlated with the severity of the disease (Banchereau and Pascual, 2006; Hahn, 1998). Perhaps unsurprisingly, IRF7, a downstream effector of both RLR and TLR signaling, has been linked to SLE onset (Xu et al., 2012). Lastly, the involvement of the ubiquitin regulatory TRIM proteins in various autoimmune and autoinflammatory disorders (including multiple sclerosis, SLE, and Sjögren's syndrome) has been established (Jefferies et al., 2011). How these negative regulatory mechanisms are disrupted in various pathological states is critical to the understanding of conditions involving chronic antiviral and inflammatory responses.

EXPERIMENTAL PROCEDURES

Plasmid Construction

Plasmids encoding GFP-MAVS, MYC-MAVS, GFP-ΔRIG-I, GFP-TBK1, GFP-IRF-3(5D), ISRE-luciferase, pRLTK, FLAG-NEMO, FLAG-TRAF3, HA-Ub,

MYC-HOIP, and HA-HOIL-1 were previously described (Paz et al., 2009, 2011; Tokunaga et al., 2009; Zhao et al., 2007). The Mda5 expression plasmid was a gift from I. Julkunen (Sirén et al., 2006). To generate GFP-Mda5 expression plasmid, Mda5 cDNA was amplified by PCR from Mda5 expression plasmid and cloned into pEGFPc1. Flag NEMO was inserted into pMSCV puro vector (Clontech). FLAG-NEMO-Ub1, Ub2, and Ub4 were constructed by adding one ubiquitin or tandem linkage of two or four ubiquitin moieties at the C terminus of Flag NEMO. To generate S-NEMO, S-NEMO-Ub1, and S-NEMO-Ub2 expression plasmids, the cDNA encoding S-NEMO, S-NEMO-Ub1, and S-NEMO-Ub2 were cloned into pTriEX-4 Neo vector (Novagen).

Cell Culture, Transfection, and Luciferase Assay

WT MEFs and *cpdm* MEFs from mice deficient in SHARPIN have been described (Gerlach et al., 2011; Ikeda et al., 2011; Tokunaga et al., 2011). HEK293 and MEFs were grown in DMEM media (Wisent) supplemented with 10% (vol/vol) FBS, L-glutamine, and antibiotics (Wisent). For luciferase assays, MEF cells grown to subconfluency in DMEM (Wisent) supplemented with 10% (vol/vol) FBS, L-glutamine, and antibiotics were transfected with 200 ng of pRLTK reporter (renilla luciferase; internal control); 200 ng of ISRE-Luc, NF-κB-Luc, IFNB-pGL3, or IFNA4-pGL3 luciferase reporter (firefly luciferase; experimental reporter); and 200 ng of MAVS, ΔRIG-I, TRIF, TBK1, or IRF-3(5D) expression plasmid using Lipofectamine 2000 according to the manufacturer's instructions (Invitrogen). HEK293 cells were transfected with 50 ng of PRLTK reporter, 100 ng of ISRE-Luc or NF-κB-Luc reporter, expression-plasmid-encoding Mda5 (200 ng), ΔRIG-I (200 ng), MAVS (50 ng), TRIF (50 ng), TBK1 (50 ng), or IRF-3 (5D) (50 ng), together with 400 ng of empty vector, LUBAC (HOIL-1 and HOIP), NEMO-Ub1, NEMO-Ub2, or NEMO-Ub4 expression plasmid by the calcium phosphate transfection method (Zhao et al., 2007). At 24 hr after transfection, luciferase activity was measured with a dual-luciferase reporter assay system according to the manufacturer's instructions (Promega). Some cells were treated with SeV (40 hemagglutination units per ml, Charles River).

Generation of Flag-NEMO, Flag-NEMO-Ub1, and Flag-NEMO-Ub2 Expressing Cell Lines

Plasmids Flag pMSCV puro, Flag-NEMO pMSCV puro, Flag-NEMO-Ub1 pMSCV puro, and Flag-NEMO-Ub2 pMSCV puro were introduced into HEK293 cells by the calcium phosphate method. Cells were selected beginning at 48 hr for approximately 2 weeks in DMEM containing 10% FBS, L-glutamine, antibiotics, and 2 μg/ml puromycin (Sigma).

Short-Interfering RNA

For siRNA experiments, siRNA-targeting human HOIL-1L (RBCK1) (Smartpool, Dharmacon), and control nontargeting siRNA pool (Dharmacon) were transfected in A549 or HEK293 cells using Lipofectamine 2000 according to the manufacturer's instructions (Invitrogen). Forty-eight hours after transfection, A549 cells were infected with SeV and harvested 4, 8, and 12 hr later. Luciferase reporter gene assays were performed on siRNA control and siRNA HOIL-1L HEK293 cells, as described above.

Immunoblot Analysis

Whole-cell lysates (40 μg) were separated by 10% SDS-PAGE. After electrophoresis, proteins were transferred for 1 hr at 4°C to nitrocellulose membranes (0.45 μ, Bio-Rad) in a buffer containing 30 mM Tris, 200 mM glycine, and 20% (vol/vol) methanol. Membranes were blocked for 1 hr at 25°C in 5% (WT/vol) dried milk in PBS and 0.1% (vol/vol) Tween-20 (PBST) and then were probed with antibody to the Flag-tag (anti Flag [M2]; Sigma Aldrich), VSV whole virus antisera, SeV antisera, anti NEMO (DA10-12; Cell Signaling), anti-HOIL-1L (RBCK1, a gift from H.-B. Shu, Wuhan University) (Zhang et al., 2008a) antibody to IRF-3 phosphorylated at Ser396 (EMD-Millipore), anti-MYC (Sigma), anti-HA (Sigma), anti-SHARPIN (Ikeda et al., 2011), anti-RIG-I (EMD-Millipore), anti-TRAF3(Santa Cruz Biotechnology), and anti-actin (EMD-Millipore) at a dilution of 1 μg/ml in 5% (WT/vol) milk in PBS. After three 10 min washes with 0.1% (vol/vol) Tween-20 in PBS, membranes were incubated for 1 hr with horseradish peroxidase-conjugated goat anti-rabbit or anti-mouse (Amersham) at a dilution of 1:3000 in blocking solution. The reaction was then visualized with an enhanced chemiluminescence detection system as recommended by the manufacturer (PerkinElmer). Densitometry analysis was performed using ImageJ software (NIH Windows version).

Protein-Protein Interaction Analysis

For S-tag precipitation, 500 μg of whole-cell lysate was incubated with 90 μl bed volume of S-protein agarose (Novagen), rotating at 4°C for 6 hr, then washed 3 times with 1 ml lysis buffer (20mM Tris [pH 7.5], 150mM NaCl, 10% glycerol, 1% triton, 1 mM DTT, 1 mM PMSF, 40 mM β-glycerol phosphate, 1 mM sodium orthovanadate, Protease inhibitor, 5 mM sodium fluoride, 10 mM N-ethylmaleimide). Washed beads were eluted by resuspension in 45 μl Laemmli Sample Buffer with β-mercaptoethanol, followed by boiling for 10 min. Eluates were electrophoresed in a 10% SDS polyacrylamide gel and transferred onto nitrocellulose blot. The transferred blots were autoclaved for 30 min in water then 15 min dry. Blots were blocked for 1 hr at room temperature in 20% heat inactivated bovine calf serum-TBS-0.45% Tween then processed for immunoblot analysis with the appropriate antibodies, as described above.

For endogenous immunoprecipitation experiments in MEFs, cells were harvested and lysed in immunoprecipitation lysis buffer (20 mM Tris [pH 7.0], 250 mM NaCl, 3 mM EDTA, 3 mM EGTA, 0.5% NP-40, 1 mM DTT, 1 mM PMSF, 40 mM β-glycerol phosphate, 1 mM sodium orthovanadate, Protease inhibitor, 5 mM sodium fluoride, 10 mM N-ethylmaleimide). To detect the ubiquitinated form of NEMO, lysed cells were incubated at 95°C for 30 min in 1% SDS in immunoprecipitation lysis buffer and then diluted to 0.1% SDS with immunoprecipitation lysis buffer. NEMO was immunoprecipitated using an antibody against NEMO (BD pharmingen) at 4°C for 2 hr, followed by incubation with protein A/G-PLUS agarose beads overnight. MAVS was immunoprecipitated using an antibody against MAVS (EMD Millipore 06-1043); TRAF3 was immunoprecipitated using an antibody against TRAF3 (Santa-Cruz, sc-6933). Immunoprecipitates were resolved on 10% SDS-PAGE and processed for immunoblot analysis with the appropriate antibodies, as described above.

Virus Production, Quantification, and Infection

Recombinant VSV-GFP, which harbors the methionine 51 deletion in the matrix protein-coding sequence (Stojdl et al., 2003), was kindly provided by J. Bell (Ottawa Health Research Institute). Virus stocks were grown in Vero cells, concentrated from cell-free supernatants by centrifugation, and titrated by standard plaque assay. Cells were infected with VSV in a small volume of medium without FBS for 1 hr at 37°C; cells were then incubated in complete medium for the indicated period of time prior to analysis. To evaluate MEF infectivity, cells were infected at different MOI with VSV-GFP. GFP fluorescence intensity was measured by flow cytometry using a FACSCalibur (BD Biosciences) and data were analyzed with FCS Express 3 (De Novo Software). IFNα, IFNβ, and IL6 in cell supernatants were quantified by ELISA (PBL Interferon Source).

Quantitative Real-Time PCR

DNase-treated total RNA from MEFs was prepared using the RNeasy kit (QIAGEN). RNA concentration was determined by absorption at 260 nm, and RNA quality was ensured by a 260/280 ratio ≥2.0. Total RNA was reverse transcribed with 100 U of Superscript II Plus RNase H reverse transcriptase using oligo AnCT primers (GIBCO BRL Life Technologies). qPCR assays were performed using the SYBR Green I on a Light Cycler apparatus (Roche Diagnostics). Murine primers sequences used in this study are as follows: *IRF-7 Forward:* 5′-AAG CAT TTC GGT CGT AGG G-3′; *IRF-7 Reverse:* 5′-GAG CCC AGC ATT TTC TCT TG-3′; *DDX58* (RIG-I) *Forward:* 5′-AAG CAA GGC TGA TGA GGA TG-3′; *DDX58* (RIG-I) *Reverse:* 5′-CTC GCA ATG TTG TAC CCA AG-3′; *OAS1 Forward:* 5′-GGC TGA AGA GGC TGA TGT GT-3′; *OAS1 Reverse:* 5′-ACC AAG CGT GTG TTC TTT CC-3′; *IL6 Forward:* 5′-CCA CGG CCT TCC CTA CTT C-3′; *IL6 Reverse:* 5′-TTG GGA GTG GTA TCC TCT GTG A-3′; *GAPDH Forward:* 5′-GGG AAG CCC ATC ACC ATC T-3′; *GAPDH Reverse:* 5′-CGG CCT CAC CCC ATT TG-3′. PCR efficiency results were obtained from duplicate measurements of two individual cDNA samples. Experiments were performed at least twice. All data are presented as a relative quantification, based on the relative expression of target genes versus *GAPDH* as reference gene and analyzed using Prism 5 software.

ACKNOWLEDGMENTS

The authors wish to thank I. Julkunen and H.B. Shu for reagents used in this study, and members of the Molecular Oncology Group at the Lady Davis Institute for helpful discussions. This research was supported by grants from Canadian Institutes of Health Research, the Terry Fox Foundation, and the Ministère du Développement économique, de l'Innovation et de l'Exportation (to R.L. and J.H.).

Received: December 22, 2011
Revised: April 30, 2012
Accepted: June 14, 2012
Published: August 15, 2012

REFERENCES

Arimoto, K., Takahashi, H., Hishiki, T., Konishi, H., Fujita, T., and Shimotohno, K. (2007). Negative regulation of the RIG-I signaling by the ubiquitin ligase RNF125. Proc. Natl. Acad. Sci. USA *104*, 7500–7505.

Banchereau, J., and Pascual, V. (2006). Type I interferon in systemic lupus erythematosus and other autoimmune diseases. Immunity *25*, 383–392.

Barrat, F.J., and Coffman, R.L. (2008). Development of TLR inhibitors for the treatment of autoimmune diseases. Immunol. Rev. *223*, 271–283.

Belgnaoui, S.M., Paz, S., and Hiscott, J. (2011). Orchestrating the interferon antiviral response through the mitochondrial antiviral signaling (MAVS) adapter. Curr. Opin. Immunol. *23*, 564–572.

Bergink, S., and Jentsch, S. (2009). Principles of ubiquitin and SUMO modifications in DNA repair. Nature *458*, 461–467.

Beutler, B.A. (2009). TLRs and innate immunity. Blood *113*, 1399–1407.

Bhoj, V.G., and Chen, Z.J. (2009). Ubiquitylation in innate and adaptive immunity. Nature *458*, 430–437.

Chariot, A., Leonardi, A., Muller, J., Bonif, M., Brown, K., and Siebenlist, U. (2002). Association of the adaptor TANK with the I kappa B kinase (IKK) regulator NEMO connects IKK complexes with IKK epsilon and TBK1 kinases. J. Biol. Chem. *277*, 37029–37036.

Dikic, I., and Dötsch, V. (2009). Ubiquitin linkages make a difference. Nat. Struct. Mol. Biol. *16*, 1209–1210.

Dixit, E., Boulant, S., Zhang, Y., Lee, A.S., Odendall, C., Shum, B., Hacohen, N., Chen, Z.J., Whelan, S.P., Fransen, M., et al. (2010). Peroxisomes are signaling platforms for antiviral innate immunity. Cell *141*, 668–681.

Gack, M.U., Shin, Y.C., Joo, C.H., Urano, T., Liang, C., Sun, L., Takeuchi, O., Akira, S., Chen, Z., Inoue, S., and Jung, J.U. (2007). TRIM25 RING-finger E3 ubiquitin ligase is essential for RIG-I-mediated antiviral activity. Nature *446*, 916–920.

Gallastegui, N., and Groll, M. (2010). The 26S proteasome: assembly and function of a destructive machine. Trends Biochem. Sci. *35*, 634–642.

Gateva, V., Sandling, J.K., Hom, G., Taylor, K.E., Chung, S.A., Sun, X., Ortmann, W., Kosoy, R., Ferreira, R.C., Nordmark, G., et al. (2009). A large-scale replication study identifies TNIP1, PRDM1, JAZF1, UHRF1BP1 and IL10 as risk loci for systemic lupus erythematosus. Nat. Genet. *41*, 1228–1233.

Gerlach, B., Cordier, S.M., Schmukle, A.C., Emmerich, C.H., Rieser, E., Haas, T.L., Webb, A.I., Rickard, J.A., Anderton, H., Wong, W.W., et al. (2011). Linear ubiquitination prevents inflammation and regulates immune signalling. Nature *471*, 591–596.

Guiducci, C., Gong, M., Xu, Z., Gill, M., Chaussabel, D., Meeker, T., Chan, J.H., Wright, T., Punaro, M., Bolland, S., et al. (2010). TLR recognition of self nucleic acids hampers glucocorticoid activity in lupus. Nature *465*, 937–941.

Häcker, H., Tseng, P.H., and Karin, M. (2011). Expanding TRAF function: TRAF3 as a tri-faced immune regulator. Nat. Rev. Immunol. *11*, 457–468.

Hahn, B.H. (1998). Antibodies to DNA. N. Engl. J. Med. *338*, 1359–1368.

Ikeda, F., Crosetto, N., and Dikic, I. (2010). What determines the specificity and outcomes of ubiquitin signaling? Cell *143*, 677–681.

Ikeda, F., Deribe, Y.L., Skånland, S.S., Stieglitz, B., Grabbe, C., Franz-Wachtel, M., van Wijk, S.J., Goswami, P., Nagy, V., Terzic, J., et al. (2011). SHARPIN forms a linear ubiquitin ligase complex regulating NF-κB activity and apoptosis. Nature *471*, 637–641.

Inn, K.S., Gack, M.U., Tokunaga, F., Shi, M., Wong, L.Y., Iwai, K., and Jung, J.U. (2011). Linear ubiquitin assembly complex negatively regulates RIG-I- and TRIM25-mediated type I interferon induction. Mol. Cell *41*, 354–365.

Jefferies, C., Wynne, C., and Higgs, R. (2011). Antiviral TRIMs: friend or foe in autoimmune and autoinflammatory disease? Nat. Rev. Immunol. *11*, 617–625.

Kato, H., Takeuchi, O., Sato, S., Yoneyama, M., Yamamoto, M., Matsui, K., Uematsu, S., Jung, A., Kawai, T., Ishii, K.J., et al. (2006). Differential roles of MDA5 and RIG-I helicases in the recognition of RNA viruses. Nature *441*, 101–105.

Kawai, T., Takahashi, K., Sato, S., Coban, C., Kumar, H., Kato, H., Ishii, K.J., Takeuchi, O., and Akira, S. (2005). IPS-1, an adaptor triggering RIG-I- and Mda5-mediated type I interferon induction. Nat. Immunol. *6*, 981–988.

Kayagaki, N., Phung, Q., Chan, S., Chaudhari, R., Quan, C., O'Rourke, K.M., Eby, M., Pietras, E., Cheng, G., Bazan, J.F., et al. (2007). DUBA: a deubiquitinase that regulates type I interferon production. Science *318*, 1628–1632.

Kirisako, T., Kamei, K., Murata, S., Kato, M., Fukumoto, H., Kanie, M., Sano, S., Tokunaga, F., Tanaka, K., and Iwai, K. (2006). A ubiquitin ligase complex assembles linear polyubiquitin chains. EMBO J. *25*, 4877–4887.

Kumar, H., Kawai, T., and Akira, S. (2011). Pathogen recognition by the innate immune system. Int. Rev. Immunol. *30*, 16–34.

Li, S., Zheng, H., Mao, A.P., Zhong, B., Li, Y., Liu, Y., Gao, Y., Ran, Y., Tien, P., and Shu, H.B. (2010). Regulation of virus-triggered signaling by OTUB1- and OTUB2-mediated deubiquitination of TRAF3 and TRAF6. J. Biol. Chem. *285*, 4291–4297.

Lin, R., Yang, L., Nakhaei, P., Sun, Q., Sharif-Askari, E., Julkunen, I., and Hiscott, J. (2006). Negative regulation of the retinoic acid-inducible gene I-induced antiviral state by the ubiquitin-editing protein A20. J. Biol. Chem. *281*, 2095–2103.

Liu, S., and Chen, Z.J. (2011). Expanding role of ubiquitination in NF-κB signaling. Cell Res. *21*, 6–21.

Liu, S.Y., Sanchez, D.J., and Cheng, G. (2011). New developments in the induction and antiviral effectors of type I interferon. Curr. Opin. Immunol. *23*, 57–64.

Loo, Y.M., and Gale, M., Jr. (2011). Immune signaling by RIG-I-like receptors. Immunity *34*, 680–692.

Malynn, B.A., and Ma, A. (2010). Ubiquitin makes its mark on immune regulation. Immunity *33*, 843–852.

Meylan, E., Curran, J., Hofmann, K., Moradpour, D., Binder, M., Bartenschlager, R., and Tschopp, J. (2005). Cardif is an adaptor protein in the RIG-I antiviral pathway and is targeted by hepatitis C virus. Nature *437*, 1167–1172.

Nakhaei, P., Mesplede, T., Solis, M., Sun, Q., Zhao, T., Yang, L., Chuang, T.H., Ware, C.F., Lin, R., and Hiscott, J. (2009). The E3 ubiquitin ligase Triad3A negatively regulates the RIG-I/MAVS signaling pathway by targeting TRAF3 for degradation. PLoS Pathog. *5*, e1000650.

Oshiumi, H., Miyashita, M., Inoue, N., Okabe, M., Matsumoto, M., and Seya, T. (2010). The ubiquitin ligase Riplet is essential for RIG-I-dependent innate immune responses to RNA virus infection. Cell Host Microbe *8*, 496–509.

Paz, S., Vilasco, M., Arguello, M., Sun, Q., Lacoste, J., Nguyen, T.L., Zhao, T., Shestakova, E.A., Zaari, S., Bibeau-Poirier, A., et al. (2009). Ubiquitin-regulated recruitment of IkappaB kinase epsilon to the MAVS interferon signaling adapter. Mol. Cell. Biol. *29*, 3401–3412.

Paz, S., Vilasco, M., Werden, S.J., Arguello, M., Joseph-Pillai, D., Zhao, T., Nguyen, T.L., Sun, Q., Meurs, E.F., Lin, R., and Hiscott, J. (2011). A functional C-terminal TRAF3-binding site in MAVS participates in positive and negative regulation of the IFN antiviral response. Cell Res. *21*, 895–910.

Rehwinkel, J., Tan, C.P., Goubau, D., Schulz, O., Pichlmair, A., Bier, K., Robb, N., Vreede, F., Barclay, W., Fodor, E., and Reis e Sousa, C. (2010). RIG-I detects viral genomic RNA during negative-strand RNA virus infection. Cell *140*, 397–408.

Sadler, A.J., and Williams, B.R. (2008). Interferon-inducible antiviral effectors. Nat. Rev. Immunol. *8*, 559–568.

Saha, S.K., Pietras, E.M., He, J.Q., Kang, J.R., Liu, S.Y., Oganesyan, G., Shahangian, A., Zarnegar, B., Shiba, T.L., Wang, Y., and Cheng, G. (2006). Regulation of antiviral responses by a direct and specific interaction between TRAF3 and Cardif. EMBO J. *25*, 3257–3263.

Schlee, M., and Hartmann, G. (2010). The chase for the RIG-I ligand—recent advances. Mol. Ther. *18*, 1254–1262.

Schlee, M., Roth, A., Hornung, V., Hagmann, C.A., Wimmenauer, V., Barchet, W., Coch, C., Janke, M., Mihailovic, A., Wardle, G., et al. (2009). Recognition of 5′ triphosphate by RIG-I helicase requires short blunt double-stranded RNA as contained in panhandle of negative-strand virus. Immunity *31*, 25–34.

Scott, I. (2010). The role of mitochondria in the mammalian antiviral defense system. Mitochondrion *10*, 316–320.

Sebban, H., Yamaoka, S., and Courtois, G. (2006). Posttranslational modifications of NEMO and its partners in NF-kappaB signaling. Trends Cell Biol. *16*, 569–577.

Sen, G.C., and Sarkar, S.N. (2007). The interferon-stimulated genes: targets of direct signaling by interferons, double-stranded RNA, and viruses. Curr. Top. Microbiol. Immunol. *316*, 233–250.

Seth, R.B., Sun, L., Ea, C.K., and Chen, Z.J. (2005). Identification and characterization of MAVS, a mitochondrial antiviral signaling protein that activates NF-kappaB and IRF 3. Cell *122*, 669–682.

Sirén, J., Imaizumi, T., Sarkar, D., Pietilä, T., Noah, D.L., Lin, R., Hiscott, J., Krug, R.M., Fisher, P.B., Julkunen, I., and Matikainen, S. (2006). Retinoic acid inducible gene-I and mda-5 are involved in influenza A virus-induced expression of antiviral cytokines. Microbes Infect. *8*, 2013–2020.

Smyth, D.J., Cooper, J.D., Bailey, R., Field, S., Burren, O., Smink, L.J., Guja, C., Ionescu-Tirgoviste, C., Widmer, B., Dunger, D.B., et al. (2006). A genome-wide association study of nonsynonymous SNPs identifies a type 1 diabetes locus in the interferon-induced helicase (IFIH1) region. Nat. Genet. *38*, 617–619.

Stojdl, D.F., Lichty, B.D., tenOever, B.R., Paterson, J.M., Power, A.T., Knowles, S., Marius, R., Reynard, J., Poliquin, L., Atkins, H., et al. (2003). VSV strains with defects in their ability to shutdown innate immunity are potent systemic anti-cancer agents. Cancer Cell *4*, 263–275.

Sutherland, A., Davies, J., Owen, C.J., Vaikkakara, S., Walker, C., Cheetham, T.D., James, R.A., Perros, P., Donaldson, P.T., Cordell, H.J., et al. (2007). Genomic polymorphism at the interferon-induced helicase (IFIH1) locus contributes to Graves' disease susceptibility. J. Clin. Endocrinol. Metab. *92*, 3338–3341.

Takeuchi, O., and Akira, S. (2010). Pattern recognition receptors and inflammation. Cell *140*, 805–820.

Tang, E.D., and Wang, C.Y. (2010). TRAF5 is a downstream target of MAVS in antiviral innate immune signaling. PLoS ONE *5*, e9172.

Tokunaga, F., Nakagawa, T., Nakahara, M., Saeki, Y., Taniguchi, M., Sakata, S., Tanaka, K., Nakano, H., and Iwai, K. (2011). SHARPIN is a component of the NF-κB-activating linear ubiquitin chain assembly complex. Nature *471*, 633–636.

Tokunaga, F., Sakata, S., Saeki, Y., Satomi, Y., Kirisako, T., Kamei, K., Nakagawa, T., Kato, M., Murata, S., Yamaoka, S., et al. (2009). Involvement of linear polyubiquitylation of NEMO in NF-kappaB activation. Nat. Cell Biol. *11*, 123–132.

Weissman, A.M., Shabek, N., and Ciechanover, A. (2011). The predator becomes the prey: regulating the ubiquitin system by ubiquitylation and degradation. Nat. Rev. Mol. Cell Biol. *12*, 605–620.

Wertz, I.E., O'Rourke, K.M., Zhou, H., Eby, M., Aravind, L., Seshagiri, S., Wu, P., Wiesmann, C., Baker, R., Boone, D.L., et al. (2004). De-ubiquitination and ubiquitin ligase domains of A20 downregulate NF-kappaB signalling. Nature *430*, 694–699.

Wilkins, C., and Gale, M., Jr. (2010). Recognition of viruses by cytoplasmic sensors. Curr. Opin. Immunol. *22*, 41–47.

Xu, L.G., Wang, Y.Y., Han, K.J., Li, L.Y., Zhai, Z., and Shu, H.B. (2005). VISA is an adapter protein required for virus-triggered IFN-beta signaling. Mol. Cell *19*, 727–740.

Xu, W.D., Zhang, Y.J., Xu, K., Zhai, Y., Li, B.Z., Pan, H.F., and Ye, D.Q. (2012). IRF7, a functional factor associates with systemic lupus erythematosus. Cytokine *58*, 317–320.

Yoneyama, M., and Fujita, T. (2008). Structural mechanism of RNA recognition by the RIG-I-like receptors. Immunity *29*, 178–181.

Yoneyama, M., and Fujita, T. (2010). Recognition of viral nucleic acids in innate immunity. Rev. Med. Virol. *20*, 4–22.

Yoneyama, M., Kikuchi, M., Natsukawa, T., Shinobu, N., Imaizumi, T., Miyagishi, M., Taira, K., Akira, S., and Fujita, T. (2004). The RNA helicase RIG-I has an essential function in double-stranded RNA-induced innate antiviral responses. Nat. Immunol. *5*, 730–737.

Zeng, W., Sun, L., Jiang, X., Chen, X., Hou, F., Adhikari, A., Xu, M., and Chen, Z.J. (2010). Reconstitution of the RIG-I pathway reveals a signaling role of unanchored polyubiquitin chains in innate immunity. Cell *141*, 315–330.

Zhang, M., Tian, Y., Wang, R.P., Gao, D., Zhang, Y., Diao, F.C., Chen, D.Y., Zhai, Z.H., and Shu, H.B. (2008a). Negative feedback regulation of cellular antiviral signaling by RBCK1-mediated degradation of IRF3. Cell Res. *18*, 1096–1104.

Zhang, M., Wu, X., Lee, A.J., Jin, W., Chang, M., Wright, A., Imaizumi, T., and Sun, S.C. (2008b). Regulation of IkappaB kinase-related kinases and antiviral responses by tumor suppressor CYLD. J. Biol. Chem. *283*, 18621–18626.

Zhao, T., Yang, L., Sun, Q., Arguello, M., Ballard, D.W., Hiscott, J., and Lin, R. (2007). The NEMO adaptor bridges the nuclear factor-kappaB and interferon regulatory factor signaling pathways. Nat. Immunol. *8*, 592–600.